Enhanced Performance of Zirconium-Doped Ceria Catalysts for the Methoxycarbonylation of Anilines

José Luis Núñez-Rico[+],[a, b] Marcos Rellán-Piñeiro[+],[b] Begoña Puértolas[+],[c] Anton Vidal-Ferran,*[a, b, d, e] Núria López,*[b] Javier Pérez-Ramírez,*[c] and Stefan Wershofen[f]

Abstract: The methoxycarbonylation of anilines stands as an attractive method for the phosgene-free production of carbamates. Despite the high yields obtained for ceria catalysts, the reduction of the amount of side products and the prevention of catalyst deactivation still represent major hurdles in this chemistry. One advantage of ceria is the possibility of tuning its reactivity by doping its lattice with other metals. In the present work, a series of doped ceria-based materials, prepared by substitution with metals, are evaluated in the methoxycarbonylation of 2,4-diaminotoluene with dimethyl carbonate. Among all catalysts, containing Eu, Hf, La, Pr, Sm, Tb, Y or Zr, ceria promoted with 2 mol% Zr exhibited 96% selectivity towards the desired carbamates, improving the pure CeO_2 catalyst. Density functional theory demonstrates that two descriptors are needed: 1) a geometric factor that governs the reduction of energy barriers for carbamate formation through ureas; 2) catalyst basicity as N–H bonds need to be activated. Assessment in subsequent reaction cycles revealed that the CeO_2–ZrO_2 catalyst is more stable than bulk CeO_2, along with the reduction of fouling processes.

Introduction

The development of efficient, green and sustainable methods for preparing carbamates is an active field of research in industry and academia due to their extensive use in the production of commodity (e.g. herbicides and pesticides) as well as specialty chemicals (building blocks for the life-science sector).[1] Their cleavage into isocyanates provides a means for the production of polyurethanes with a market size of ca. USD 66 billion in 2018.[2] Although currently there are no alternative technologies available to phosgenation for manufacturing aromatic isocyanates such as TDI (2,4-diisocyanato-1-methylbenzene) and MDI (bis(4-isocyanatophenyl)methane), a plethora of catalytic methods for transforming anilines into the corresponding carbamates by alkoxycarbonylation have been reported in the literature. Preparation methods based on homogeneous catalysts are mostly governed by Zn-based materials[3] that, despite providing higher conversions and selectivities, their recovery and re-use is difficult. These issues can be overcome by the use of heterogeneous systems (supported $Zn(OAc)_2$,[4] CeO_2,[5] $Au@CeO_2$,[6, 5b] $ZnAlPO_4$,[7] $[Zn]SiO_2$,[8] AlSBA-15,[9] $[ZnCO_3]_2{\cdot}[Zn(OH)_2]_3$,[10] $(PbCO_3)_2{\cdot}Pb(OH)_2$,[10] Bi/Yb/Ge/$SiO_2$ composite,[11] Zr-MOF-808@MCM-41,[12] Zn/Al/Ce mixed oxide[13]) at the expense of decreased yields.

CeO_2 is used as a support, stabilizer, promoter or catalyst owing to its unique structural and electronic properties.[14] It is a key ingredient of many heterogeneous catalysts for a variety of reactions, including the purification of exhaust automotive gases in three-way catalytic converters, the preferential oxidation of CO in oxygen-rich streams, the production of hydrogen in low-temperature solid fuel cells, the oxidation of HCl[15] and the high-temperature electrocatalytic water splitting reaction (WSR).[16] By combining experiment and theory, our groups reported the reaction mechanism of CeO_2 in the methoxycarbonylation of the industrially relevant aniline 2,4-**TDA** (4-methylbenzene-1,3-diamine) with **DMC** (Scheme 1).[5c] In this reaction,

[a] *Dr. J. L. Núñez-Rico,[+] Prof. A. Vidal-Ferran*
Department of Inorganic and Organic Chemistry, University of Barcelona
C. Martí i Franquès 1-11, 08028 Barcelona (Spain)
E-mail: anton.vidal@icrea.cat

[b] *Dr. J. L. Núñez-Rico,[+] Dr. M. Rellán-Piñeiro,[+] Prof. A. Vidal-Ferran, Prof. N. López*
Institute of Chemical Research of Catalonia (ICIQ) and The Barcelona Institute of Science and Technology
Avgda. Països Catalans 16, 43007 Tarragona (Spain)
E-mail: nlopez@iciq.es

[c] *Dr. B. Puértolas,[+] Prof. J. Pérez-Ramírez*
Department of Chemistry and Applied Biosciences
Institute for Chemical and Bioengineering, ETH Zurich
Vladimir-Prelog-Weg 1, 8093 Zurich (Switzerland)
E-mail: jpr@chem.ethz.ch

[d] *Prof. A. Vidal-Ferran*
Catalan Institution for Research and Advanced Studies (ICREA)
Pg. Lluís Companys 23, 08010 Barcelona (Spain)

[e] *Prof. A. Vidal-Ferran*
Institut de Nanociència i Nanotecnologia (IN2UB)
Universitat de Barcelona
08028, Barcelona (Spain)

[f] *Dr. S. Wershofen*
Covestro (Deutschland) AG
Kaiser-Wilhelm-Allee 60, 51373 Leverkusen (Germany)

[+] *These authors contributed equally to this work.*

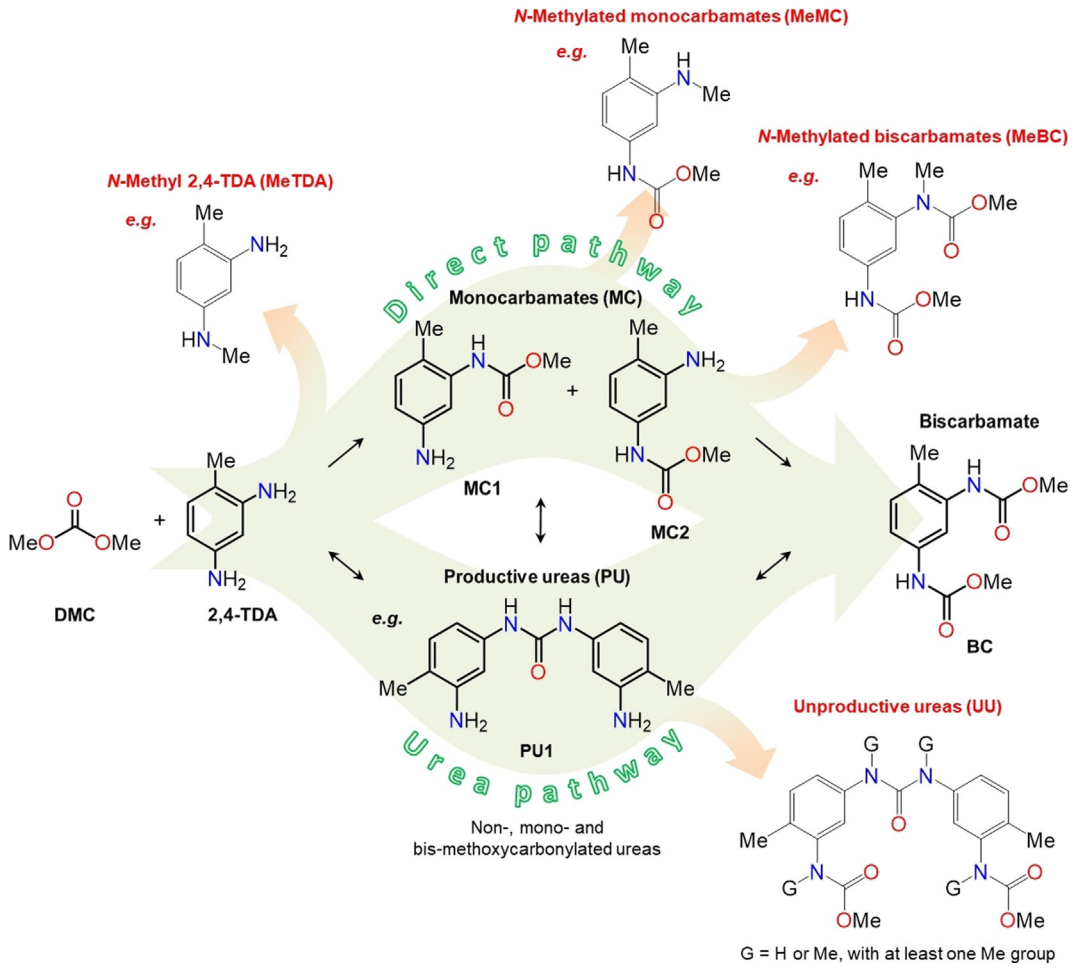

Scheme 1. Simplified reaction network of the methoxycarbonylation of 2,4-**TDA** with **DMC** employing $Ce_{1-x}M_xO_2$ as catalysts (for the detailed list of structures, see the Supporting Information).

the success of CeO_2 stems from its ability to cleave the methoxycarbonylating agent (i.e.; **DMC**) into reactive methoxycarbonyl groups that are transferred to an aromatic amino group with the formation of a carbamate. Part of these carbamates react to form productive ureas, unprecedented intermediates that can be methoxycarbonylated and reversely transformed into carbamates. Overall, our studies demonstrated that methoxycarbonylation of 2,4-**TDA** using nanocrystalline CeO_2 led to ca. 90% yield of carbamates and 10% of side products, mainly *N*-methylated carbamates and (*N*-methylated) ureas, although the formation of carbonaceous deposits along with the surface reconstruction lead to the deactivation of the catalyst upon subsequent cycles. The stability of CeO_2 has been also compromised under high-temperature conditions, as those reached in the vehicle exhaust due to particle sintering,[17] or in the oxidation of HCl as CeO_2 tends to form chlorinated species at the surface and the bulk.[18] To enhance the stability, doping of the CeO_2 by substitution of lattice Ce ions with Zr and/or other rare earth elements via the formation of solid solutions is commonly applied.[19] We hypothesized that doping ceria with alio- or isovalent metal oxides would translate into a modification of the distribution of the vacancies at the surface, which have proven to be important in the generation and subsequent transfer of the methoxycarbonyl and carbamate groups.

In this study, we have prepared, characterized and evaluated as methoxycarbonylating catalysts an array of nanocrystaline CeO_2 materials, which have been doped at different levels with a number of metal (Eu, Hf, La, Pr, Sm, Tb, Y or Zr). The efficiency of the best-performing CeO_2-ZrO_2 material has been rationalized by DFT and compared to that of pure CeO_2. Assessment of the structural stability upon subsequent cycling was also conducted.

Results and Discussion

Preparation and characterization of $Ce_{1-x}M_xO_2$ catalysts

Mixed CeO_2–M_yO_z systems ($Ce_{1-x}M_xO_2$) with metal M contents ranging from 1 to 10 mol% (i.e. $0.01 \leq x \leq 0.1$; x = molar ratio), where M stands for Eu, Hf, La, Pr, Sm, Tb, Y or Zr,[20] were prepared by the co-precipitation method in the presence of H_2O_2. XRD analysis of the $Ce_{1-x}M_xO_2$ materials with 2 and 5 mol% ($x = 0.02$ or 0.05) metal content evidenced the characteristic re-

flections of the cubic fluorite structure of CeO_2, regardless of the nature and loading of the dopant (Figures S1 and S2). In all cases, the peaks were relatively broad, suggesting their small particle size, which is in line with the crystallite size estimated by the Scherrer equation (≈10 nm). The total surface area ranged from 67 to 75 $m^2 g^{-1}$, which was comparable to that of the bulk CeO_2 prepared by precipitation (S_{BET} = 70 $m^2 g^{-1}$). HRTEM of the catalyst with 2 mol% zirconium content revealed the presence of irregularly shaped polyhedral particles of variable diameter (10–40 nm), whose dominant lattice fringes (0.31 nm) corresponded to the (111) facet (Figure 1). Energy-

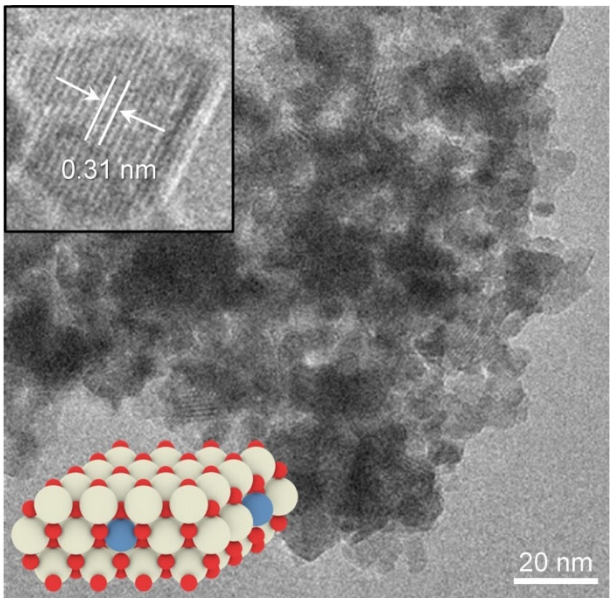

Figure 1. HRTEM of $Ce_{0.98}Zr_{0.02}O_2$ in fresh form. The inset corresponds to the perspective view of the (111) surface. Color code: Ce (cream), O (red), Zr (blue).

dispersive X-ray spectroscopy (EDS) chemical mapping evidenced the homogeneous distribution of zirconium over the CeO_2 particles (Figure 2).

Catalytic evaluation of $Ce_{1-x}M_xO_2$

$Ce_{1-x}M_xO_2$ catalysts with a metal M content of 2 and 5% were evaluated in the methoxycarbonylation of 2,4-**TDA** with **DMC**, both as reagent and solvent (30 equiv of DMC with respect to 2,4-**TDA**), under standard screening conditions for this chemistry: 20 m^2 per mmol of 2,4-**TDA**, 413 K, 7.5 h (see Experimental Section for details). A summary of the results obtained is shown in Figure 3 and Table S1. Whilst Pr- and Sm-doped ceria showed the same activity as CeO_2 (83% of **BC** and 90% of combined yield, **MC1** + **MC2** + **BC**), the rest of the doped systems evidenced higher selectivity to carbamates. The Zr-doped ceria with 2 mol% Zr showed the best performance in the methoxycarbonylation of 2,4-**TDA** (96% combined yield of carbamates), whilst combined yields ranging from 92 to 93% were observed for the rest of the other ceria-doped materials. For instance, Eu- and Hf-doped materials evidenced 93% combined yield of carbamates and higher amounts of not fully methoxycarbonylated 2,4-**TDA**, that is, ≥10% of **MC1** plus **MC2** in

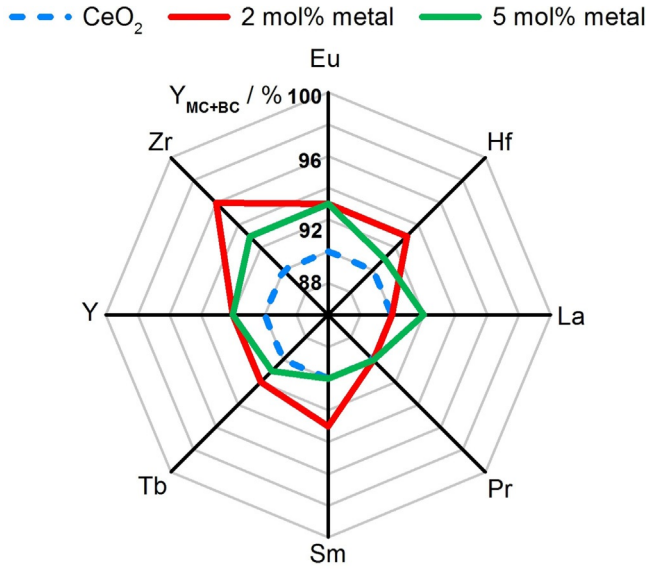

Figure 3. Plot of the combined yield of mono- and biscarbamates using $Ce_{1-x}M_xO_2$ with 2 mol% metal (green line) or 5 mol% metal (red line) as catalysts in the methoxycarbonylation of 2,4-**TDA** with **DMC**. Dotted blue line represent the results obtained for CeO_2.

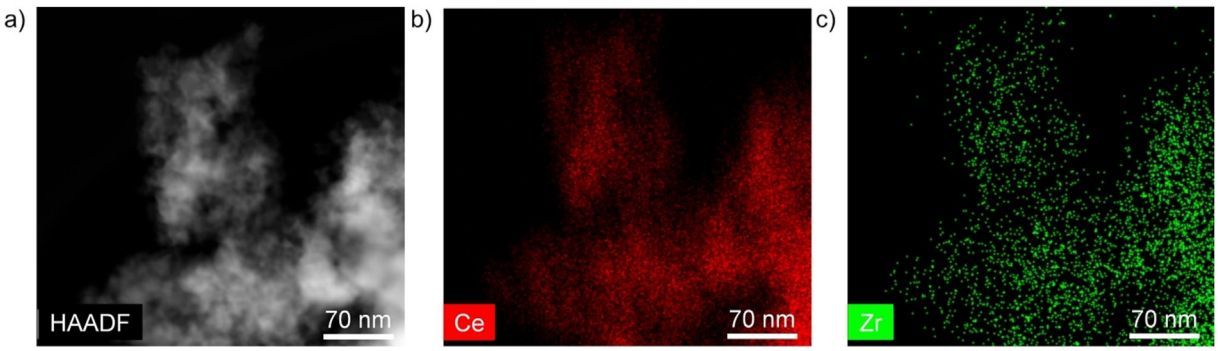

Figure 2. HAADF STEM images (left) and elemental maps (middle and right) of Ce (red) and Zr (green) of the $Ce_{0.98}Zr_{0.02}O_2$ catalyst.

contrast to the Zr-doped material for which only 8% of **MC1** plus **MC2** was detected.

The impact of different contents of Zr, i.e., $0 < x \leq 0.1$, with x being molar ratio of Zr, on the catalytic performance was studied. The results showed a maximum in **BC** and combined yields for the sample with 2 mol% ($x = 0.02$) Zr loading (88 and 96%, respectively). Increasing amounts of Zr led to a lower yield of BC (78% at $x = 0.1$) than that obtained using pure CeO_2. The activity towards methoxycarbonylation decreased with the increase of Zr loading as the amounts of not fully methoxycarbonylated 2,4-**TDA** increased and, thus, the combined yield of **MC1** and **MC2** increased. The formation of undesired *N*-alkylated carbamates (see Scheme 1 for the structures) is not affected by the Zr doping level as the same amount was detected regardless the Zr loading (Figure 4). Similarly, the amount of productive ureas detected at the end of the reaction was also independent of the Zr doping level (contents < 1 mol%). In contrast, the amounts of unproductive ureas (see Scheme 1 for the structures) showed a minimum yield of ca. 2% for the best-performing material ($Ce_{0.98}Zr_{0.02}O_2$). Higher Zr loadings led to increased amounts of unproductive ureas (ca. 4% yield of unproductive ureas with the $Ce_{0.9}Zr_{0.1}O_2$ catalyst, Figure 4).

When $Ce_{0.98}Zr_{0.02}O_2$ was used as catalyst, the substrate was fully converted and 88% of **BC** and 8% of the mixture of **MC1** and **MC2** were formed (Scheme 1). Along with the desired products, ca. 7 mol% of side products (3 mol% of *N*-methylated carbamates, ca. 3 mol% of (*N*-methylated) ureas and less than 1 mol% of unidentified compounds) were also detected in the final methoxycarbonylation reaction mixture.[21] Thus, by using $Ce_{0.98}Zr_{0.02}O_2$, the selectivity towards the desired compounds increased by 6% and the formation of side products diminished by 2% with respect to the reference CeO_2 material. The results with $Ce_{0.98}Zr_{0.02}O_2$ were reproducible and the standard deviation values for the yields of **MC1**, **MC2**, and **BC** after 6 independent runs were ca. 1% for **BC** and ca. 1% for the sum of **MC1** and **MC2**.

In this complex reaction scenario, 2,4-**TDA** was first converted to monocarbamates (**MC1** or **MC2**), which then underwent a second methoxycarbonylation reaction at longer reaction times towards the final **BC** product (direct pathway; Scheme 1). Along with this path, monocarbamates reacted with themselves or with 2,4-**TDA** to form urea-containing compounds (i.e.; the so called productive ureas), which can be methoxycarbonylated and further evolved to the desired biscarbamate **BC** by cleavage with MeOH in the presence of the catalyst (urea pathway; Scheme 1). The important amounts of productive ureas detected in the reaction mixture (ca. 12 mol% of non-methoxycarbonylated ureas such as **PU1** and its positional isomers[21] at 15 min, ca. 8 mol% of the mono(methoxycarbonylated) analogues of **PU1** and their positional isomers[21] at ca. 50 min and ca. 6 mol% of bis(methoxycarbonylated) analogues of **PU1** and their positional isomers[21] at ca. 100 min; see Figure 5a) highlight the relevance of the urea pathway in the overall transformation of 2,4-**TDA** into **BC**.

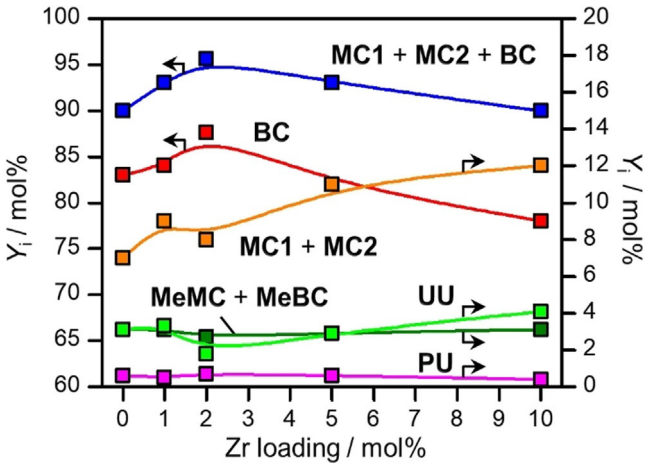

Figure 4. Combined yield of carbamates (blue line), yield of **BC** (red line), yield of **MC1** + **MC2** (orange line), yield of *N*-methylated carbamates (dark green line), yield of unproductive ureas (light green line) and yield of productive ureas (pink line) versus the zirconium content for $Ce_{1-x}Zr_xO_2$ catalysts.

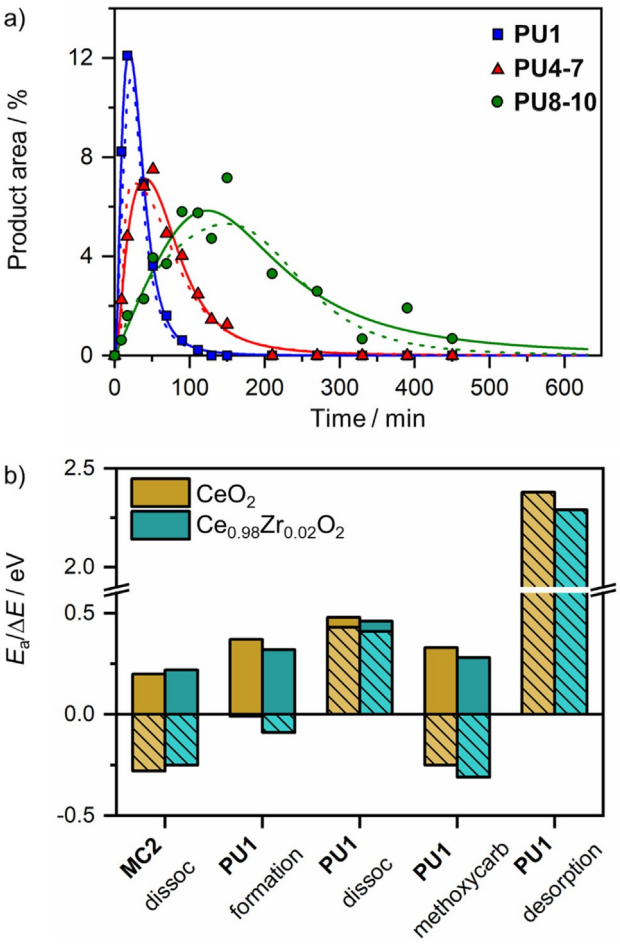

Figure 5. (a) Concentration profiles of productive ureas as a function of reaction time. Solid lines represent the results obtained with $Ce_{0.98}Zr_{0.02}O_2$ and dotted lines those obtained with CeO_2. Lines correspond to eye guidelines. (b) Energies of the involved processes in the production of ureas. Plain bars represent activation energies, E_a, and stripped bars represent reaction energies, ΔE.

Role of zirconium as selectivity enhancer

The effect of Zr doping on the product distribution was rationalized by means of DFT. The reaction mechanism previously reported for the methoxycarbonylation of 2,4-**TDA** with **DMC** over CeO_2 was simulated on the Zr-doped CeO_2(111) surface,[5c] as this surface is the only one exposed to the reagents in the fresh material, Figure 1. In the coprecipitation synthetic protocol, the final distribution of Zr atoms (either surface or subsurface position) depends on the segregation energy, which for the CeO_2(111) facet is 0.12 eV more stable for Zr being located in subsurface (and bulk) positions, in agreement with previous studies.[22] Accordingly, the Boltzmann distribution indicates that at 298 K (the material is synthesized at room temperature) around 99% of Zr atoms are placed in subsurface (or bulk) positions. Moreover, EDS chemical mapping evidenced the high degree of dispersion of Zr over the bulk CeO_2 (Figure 2). Thus, the mechanism was assessed in supercells with a single Zr atom replacing a subsurface Ce atom. Both Ce and Zr have the same oxidation states and therefore, this substitution constitutes an isovalent doping.[23]

The introduction of Zr atoms in subsurface positions does not produce changes in the reaction steps previously described for the pristine CeO_2(111) surface. They were simulated on surface positions next to the Zr atom, where small structural (bond lengths) and electronic (Bader atom charges) differences were found[23] (Table S2). The direct pathway on the Zr-doped surface (Scheme 1) has slightly smaller adsorption energies with respect to pristine CeO_2(111) (Figure S3 and Table S3). Adsorption energies of **DMC** and carbamates through the C=O group, which interacts with a Ce–O_{latt} unit forming C–O_{latt} and O–Ce bonds, are about 0.1 eV smaller on the doped surface than on pristine CeO_2(111) due to the combination of shorter Ce–O_{latt} bonds (by 0.02 Å in the clean surfaces, Table S2) and slightly smaller positive charge density on the Ce atoms (Bader charges are 2.39 and 2.37 $|e^-|$ in reactive Ce centers for pure and Zr-doped CeO_2, respectively, Table S2). Adsorption of 2,4-**TDA** and carbamates through the amino group on Ce cations results in adsorption energies $\approx$0.02 eV smaller than on the undoped CeO_2 surface (the difference is small, but a clear trend is observed) due to the smaller positive charge of the Ce cations in the doped system. On the other hand, a systematic decrease of 0.02 eV in the activation and reaction energies for -NH_2 dissociation steps is observed. For methoxycarbonylation reactions, values for activation and reaction energies are very similar to those described for pure CeO_2 and no clear trends are obtained (Figure S3 and Table S3). Reaction energy profile is shown in Figure S4.

In addition to the direct pathway, the final product can be formed through the intermediacy of urea derivatives, as described above, which are cleaved into carbamates by methanol in the presence of the catalyst (urea pathway, Scheme 1). Ureas are formed by the condensation of the activated amino group of 2,4-**TDA** (or monocarbamates) with the carbamate group of monocarbamates (or biscarbamate). The adsorption energies of these compounds through amino or C=O groups follow the same trends described for the main path. However, the activation energies for urea formation (0.32 eV) and the methoxycarbonylation of these urea derivatives (0.28 eV) are 0.05 eV lower than in the undoped system (activation energies of 0.37 and 0.33 eV for urea formation and urea methoxycarbonylation, respectively, on the pristine CeO_2(111) surface (Figure 5b). Moreover, the thermodynamics of these condensation steps is slightly favored on the Zr-containing ceria being 0.08 and 0.06 eV more exothermic for the urea formation and methoxycarbonylation, respectively. Thus, the thermodynamic equilibrium is displaced by a factor of 9.5 and 5.4, respectively, towards the condensation products (Figure 5b) and thus the urea pathway is promoted on this system. The enhancement of the urea pathway on the doped system is linked to the shorter Ce–O_{latt} bond resulting in slightly smaller displacement of aromatic units during the C–N bond formation. Due to the large size of the ureas, this smaller displacement reduces the activation energies. Therefore, the urea reactivity is governed by a geometric descriptor.[23,24] The energy profile for urea formation and further methoxycarbonylation is shown in Figure S5. Finally, the methylation of 2,4-**TDA** and **MC2** towards the corresponding side products on the doped system was also studied. Although the activation energies are reduced on the doped catalyst to 0.80 and 0.95 eV for methylation of 2,4-**TDA** and **MC2**, respectively, they are still too high to compete with the selective mechanism.

In summary, the main difference with respect to the reactivity on the undoped CeO_2(111) is observed in the condensation pathway. Ureas are kinetic products that are mainly formed at the first stages of the reaction and are cleaved into **MC1**, **MC2** or **BC** in the presence of catalysts at longer reaction times, until they reach the thermodynamic equilibrium. DFT predicts a faster formation of ureas followed by their methoxycarbonylation and further cleavage in carbamates. These observations are in agreement with the experimental data, which evidenced higher concentrations of ureas along the reaction coordinate at earlier reaction times over the Zr-doped material (Figure 5a). Indeed, during all the catalytic process, the yields of **MC1**, **MC2**, **BC** and productive ureas were higher for the doped system. Therefore, the presence of Zr centers in the ceria accelerates the reaction rate of the urea pathway, but it has no significant effects in the direct pathway. The faster formation of ureas and methoxycarbonylation of their amino groups, which favors the formation of selective products against methylations, could explain the superior performance observed for the doped system.

Activity analysis to search for a descriptor can be done once the mechanism is understood. In our case, alio- and isovalent dopants need to be separated first since the catalytic response of 3+ cations affects many factors. For the remaining systems, the descriptors need to account for both the direct path and the condensation one (**PU**). For the ureas path, a simple geometric descriptor qualitatively indicates that the highest activity of Zr-doped catalyst is due to shorter O_{latt}–Ce bond distance; this is because of the large size of the organic fragments, which are strongly bound to the surface and, therefore, the smaller the path in the rearrangements makes the **PU** formation more effective. However, due to the delicate balance

between the direct and condensation path, this descriptor cannot explain the activity of all doped systems. As the first step in the reaction network implies the activation of the N–H bond, we have investigated the acid-base properties of the different surfaces. Particularly, the basicity of surface oxygens[25] can be theoretically measured by the O(2p) band center[23] (Table S4). Thus, a collective descriptor[24] that includes the bond distance and O(2p) band center was applied to isovalent dopants giving a good correlation with the catalytic performance (Figure S6). Therefore, in order to be successful, the dopant needs to enhance the basicity (small O(2p) value) and reduce the O_{latt}–Ce bond distance.

Reusability of the Zr-doped CeO_2 catalyst

Regarding the stability of the Zr-doped ceria with 2 mol% Zr loading, the impact of 6 consecutive catalytic cycles on the conversion and selectivity was evaluated. After each run, the catalyst was recovered and cleaned. The surface area suffered slight variations after each cycle and, therefore, the amount of catalyst was adjusted to 20 $m^2 mmol^{-1}$ of 2,4-**TDA** prior to be used in the next cycle. The results of the recyclability evaluation of $Ce_{0.98}Zr_{0.02}O_2$ have been summarized in Table 1. The catalytic performance was retained during 3 cycles and steadily decreased during the following cycles. Thus, in the 6th cycle, only 75% of 2,4-**TDA** was converted, whereas the selectivity strongly decreased to 4% of **BC** and 16% of combined yield of mono- and biscarbamates and the methylated compounds reached 38% (Table 1). Although analogous behavior was reported for the CeO_2 reference material,[5c] the activity and selectivity decreased to a lower extent in the case of the Zr-doped catalyst, as shown in Figure 6a. The yield of **BC** and the combined yield of carbamates was higher in the Zr-doped catalyst than in CeO_2 in the first 5 cycles. Moreover, although TGA analyses revealed the increased amount of carbon deposits with the number of cycles (from 13.4 wt.% after 3 cycles to 17.7 wt% after 6 cycles, Figure 6b), they were lower than those detected for the pure CeO_2 material (17.7 wt.% versus 24.1 wt.%).

The stability of $Ce_{0.98}Zr_{0.02}O_2$(111) and its possible restructuring towards (100) surface was studied since the appearance of (100) surface after several catalytic runs is related with the formation of methylated species in the CeO_2 system.[5c] This is in line with the high formation of methylated species observed experimentally over CeO_2 nanocubes,[5a] which mainly expose this face. The (100) surface has intrinsic vacancies that promote the formation of surface methyl groups O_{latt}–CH_3, which can act as methylating agents. The $Ce_{0.98}Zr_{0.02}O_2$ catalyst used after 6 cycles was examined by HRTEM, revealing the presence of the (100) surface (Figure 7a), which is indeed related with the increase of methylated carbamates and ureas observed upon recycling. The adsorption of **DMC** stabilizes the catalyst surfa-

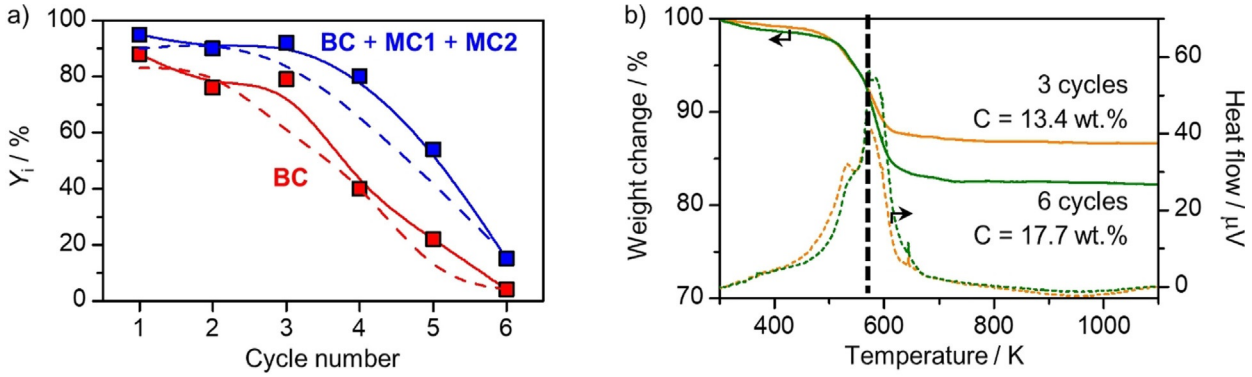

Figure 6. (a) Evolution of the yield of **BC** and combined yield of carbamates over $Ce_{0.98}Zr_{0.02}O_2$ upon consecutive cycles. Dashed lines stand for the evolution over CeO_2. (b) Thermogravimetric analysis (TGA) in air atmosphere of $Ce_{0.98}Zr_{0.02}O_2$ after being used in the methoxycarbonylation of 2,4-**TDA** with **DMC** in different cycles. The values of the 6th cycle correspond to the results after regeneration of the catalyst with **DMC**.

Table 1. Recycling results of $Ce_{0.98}Zr_{0.02}O_2$ in the methoxycarbonylation of 2,4-**TDA** with **DMC**.[a] Values are expressed as an average of at least two independent runs. The structures corresponding to each group of compounds are detailed in the Supporting Information.

Cycle	S_{BET}[b] [$m^2 g^{-1}$]	$X_{2,4\text{-TDA}}$[c] [%]	Y_{MC}[d] [%]	Y_{BC} [%]	Y_{MeTDA} [%]	**MeC**[e] [area%]	**PU** + **UU**[e] [area%]	Unknown[e] [area%]	C_{bal}[f] [%]
#1[g]	69	100	8	88	0	3	2	<1	101
#2	56	100	14	76	0	4	3	1	98
#3	56	100	13	79	0	4	2	1	99
#4	60	99	40	40	1	7	4	2	97
#5	52	98	32	22	2	12	5	3	78
#6[h]	71	75	12	4	9	29	2	9	90

[a] Reaction conditions: **DMC**:2,4-**TDA** = 30:1, catalyst loading = 20 m^2 per mmol of 2,4-**TDA**, 413 K, 7.5 h, autogenous pressure. [b] Surface area of the catalyst prior to each catalytic cycle. The weight of catalyst added to the reaction mixture was varied in the range of 0.84–1.26 g, in order to keep a fixed ratio of 20 m^2 per mmol of 2,4-**TDA**. [c] Conversion of 2,4-**TDA**. [d] Corresponds to the sum of the yields of the *para*- and *ortho*- isomers. [e] Not quantified, results are expressed as area%. [f] Sum of all the detected species.; $C_{bal} = (100\text{-}X_{TDA}) + \Sigma Y_{MC,BC,MeTDA} + \Sigma area\%_{MeMC,\ MeMC,\ PU,\ UU,\ unknown}$. [g] The results were reproducible and the standard deviation values for the yields of **MC1**, **MC2**, and **BC** after 6 independent runs were 0.4% for the sum of **MC1** and **MC2**, and 1.3% for **BC**. [h] The values of the sixth cycle correspond to the results after regeneration of the catalyst with **DMC**.

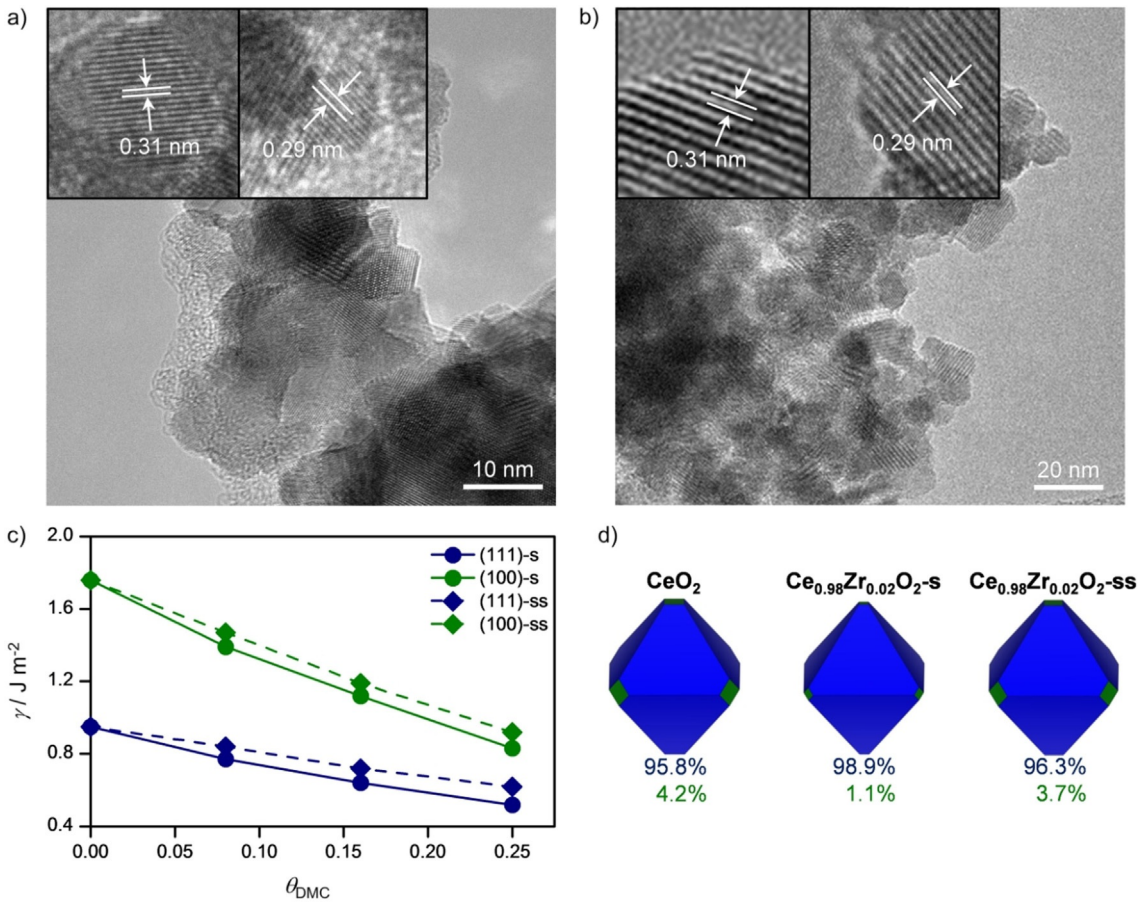

Figure 7. HRTEM of $Ce_{0.98}Zr_{0.02}O_2$ after (a) 6 consecutive cycles and (b) a 42 h treatment with **DMC**. (c) (111) and (100) surface energies as function of the time for the doped catalyst with Zr atom placed in surface (s) or subsurface (ss) layer. (d) Wulff constructions for CeO_2 and $Ce_{0.98}Zr_{0.02}O_2$ for $\theta_{DMC} = 0.25$ and percentage of each surface: (111) in blue and (100) in green.

ces and reduces the surface energy in a proportional extent to its adsorption energy. DFT simulations showed large differences for **DMC** adsorption energy on (111) and (100) surfaces, either for Zr placed in surface position (−1.59 and −3.30 eV, respectively) or subsurface position (−0.87 and −2.90 eV, respectively). Therefore, both surfaces are stabilized in a different extent resulting in a thermodynamic factor of shape control that leads to surface restructuration.[26,27] The presence of Zr at medium/low coverage does not produce significant changes in the surface energies of the clean catalyst for both surfaces with respect to CeO_2 (Figure S7) and the Wulff construction shows only the (111) facet, in line with high-resolution micrographs (Figure 1). The impact of **DMC** coverage in surface energies was simulated for Zr atoms placed in both surface and subsurface positions (Figure 7c). With Zr placed in surface layer, medium **DMC** coverage ($\theta_{DMC} = 0.25$) reduced the surface energies to 0.52 and 0.83 J m^{-2} for (111) and (100) surfaces, respectively. With Zr placed in subsurface, the effect was slightly lower and the obtained surface energies were 0.62 and 0.92 J m^{-2} for (111) and (100) surfaces, respectively. Thus, Wulff constructions at $\theta_{DMC} = 0.25$ predict a lower exposure of (100) surface; 1.1 and 3.7% of (100) surface for Zr located in surface and subsurface layer, respectively (Figure 7d). These values are lower than the 4.2% of (100) predicted for plain CeO_2. Therefore, the presence of Zr increased the catalyst stability by reducing the appearance of (100) surface, in line with the lower amount of methylated products and carbon deposits observed experimentally after several cycles. The treatment of fresh $Ce_{0.98}Zr_{0.02}O_2$ catalyst with DMC in the absence of any other compound during 42 h (the time corresponding to 6 catalytic cycles) confirmed the restructuration of the surface induced by the solvent, as shown by the (100) surface appearance in the HRTEM micrograph (Figure 7b).

Conclusions

A series of $Ce_{1-x}M_xO_2$ catalysts (M = Eu, Hf, La, Pr, Sm, Y, Zr, or Tb, $0.01 \leq x \leq 0.1$) have been prepared, characterized and assessed in the methoxycarbonylation of 2,4-**TDA** with **DMC** for the production of isocyanate precursors. Zirconium-doped CeO_2 outperforms the rest of the investigated systems in terms of the yield of **BC** and combined yield of carbamates. Among the different Zr contents studied, a Ce/Zr molar ratio of 98:2 proved to be the optimal, as higher amounts of Zr led to lower amounts of fully methoxycarbonylated 2,4-**TDA** and increased amounts of side products. Overall, the best-performing catalyst led to 96% selectivity to carbamates whereas 90% selectivity was obtained for the pure CeO_2 material. The amount of side products over this system were reduced by 2% with respect to CeO_2. The improved catalytic performance was ration-

alized by density functional theory, which evidenced a more energetically favorable path through the urea pathway than in the case of CeO_2. In general, the formation of the desired products depends on two descriptors for isovalent dopants, the basicity of the centers (ability to activate N–H bonds), promoting all the reactions, and the surface geometric factors (O_{latt}–Ce distances), which become important due to the large size of urea molecules. Recyclability tests indicated that the conversion of the substrate and the selectivity to carbamates decreased after 3 cycles, which was related to the increased formation of carbonaceous residues on the surface, thus reducing the catalyst activity, together with the surface restructuring towards the unselective (100) surface after **DMC** exposure, which reduces the catalyst selectivity. Whereas the fresh catalyst mainly exhibited the (111) facet, repeated exposure to **DMC** evidenced the occurrence of the oxygen-defective (100) facet. In line with the experimental evidences, the presence of Zr atoms on the surface and in the subsurface has been predicted to reduce the surface restructuring process with respect to the stoichiometric CeO_2, with overall decreased deactivation rate for the $Ce_{0.98}Zr_{0.02}O_2$. Our study not only identifies key aspects for the improvement of the performance of CeO_2-based catalysts through the analysis of the energetic profile of the urea pathway, but also in the phase stabilization of the (111) facet of the catalyst.

Experimental Section

Catalyst preparation and characterization: Mixed CeO_2-M_yO_2 systems ($Ce_{1-x}M_xO_2$) with metal contents of 2 and 5 mol%, where M stands for Eu, Pr, Sm, Tb, La, Y, Hf or Zr, were prepared by the co-precipitation method in the presence of H_2O_2 following a reported protocol.[29] Additional catalysts with 1 and 10 mol% Zr were prepared. In a typical synthesis, $Ce(NO_3)_3{\cdot}6H_2O$ (99.5%, Acros) was dissolved in deionized water (in a weight ratio of 1:10) under stirring at room temperature, while the metal nitrate solution ($ZrO(NO_3)_2$ (35% in diluted nitric acid, Sigma–Aldrich; $Eu(NO_3)_3{\cdot}6H_2O$, 99.9%, ABCR; $Pr(NO_3)_3{\cdot}6H_2O$, 99.9%, Sigma–Aldrich; $Sm(NO_3)_3{\cdot}6H_2O$, 99.9%, Acros Organics; $Tb(NO_3)_3{\cdot}5H_2O$, 99.9%, Sigma–Aldrich; $La(NO_3)_3{\cdot}6H_2O$, 99.999%, Acros Organics; $Y(NO_3)_3{\cdot}6H_2O$, 99.9%, ABCR) was added. For the preparation of Hf-doped CeO_2, $HfCl_4$ (99.9%, Strem Chemicals) was used as precursor. Hydrogen peroxide (35%, Sigma–Aldrich) was poured into the solution to obtain a molar H_2O_2:(Ce+M) ratio of 3:1. The precipitation was obtained by adding aqueous NH_4OH (30%, Sigma–Aldrich) until the pH equaled to 10.5. The slurry was stirred for 4 h at room temperature and the precipitate was separated by filtration, washed with deionized water, dried at 373 K in static air for 12 h and calcined at 773 K (heating rate = 5 K min^{-1}) in static air for 5 h.

Powder X-ray diffraction (XRD) was measured using a PANalytical X'Pert PRO-MPD diffractometer and Cu-Kα radiation (λ = 0.15418 nm). The diffraction data was recorded in the 10–70° 2θ range with an angular step size of 0.017° and a counting time of 0.26 s per step. N_2 sorption at 77 K was measured in a Micromeritics TriStar II analyzer. Prior to the measurement, the solid was outgassed at 573 K for 3 h. The Brunauer–Emmett–Teller (BET) method was applied to calculate the total surface area, S_{BET}, in m^2 g^{-1}. Samples for high-angle annular dark-field (HAADF) scanning transmission electron microscopy (STEM) and high-resolution transmission electron microscopy (HRTEM) studies were prepared by dusting respective powders onto carbon coated copper grids. Imaging was performed on a Talos F200X instrument operated at 200 kV and equipped with a FEI SuperX detector. The content of residues in the used catalysts was determined by thermogravimetric analysis (TGA) using a Linseis TGA PT1600 thermobalance. The solid (ca. 25 mg) was placed in an alumina crucible and heated in 5 vol.% O_2/Ar (300 cm^3 STP min^{-1}) from ambient temperature to 1173 K at 10 K min^{-1}.

Evaluation of catalytic performance and product analysis: Methoxycarbonylation reactions were performed in a 25-cm^3 stainless steel autoclave (Berghof high-pressure reactor BR-25). In a typical experiment, the catalyst was placed in the Teflon vessel along with 2,4-**TDA** (396 mg, 3.2 mmol, Sigma–Aldrich, 98%) and the required amount of dry **DMC** (8.2 cm^3, 97.2 mmol, Sigma–Aldrich, 99%, < 30 ppm final water content). The total surface area was measured prior to the reaction and the amount of catalyst was adjusted accordingly in order to keep a fixed ratio of 20 m^2 per mmol of 2,4-**TDA**. Then, the autoclave was closed, placed in an aluminum heating block and purged with N_2. Stirring was then started (810 rpm) and reaction times up to 10.5 h were studied. The temperature was controlled by a thermocouple connected to the heating plate. After the desired reaction time the autoclave was removed from the heating block and cooled down in an ice-water bath for a minimum of 30 min. The solid catalyst was then recovered by filtration and the Teflon vessel and the solid residue were washed with acetone (5 times, 5 cm^3). The combined organic fractions were collected and concentrated under vacuum to give the reaction mixture. The composition of the reaction mixture and determination of the yields of 2,4-**TDA**, **MC1**, **MC2** and **BC** was performed following an already reported method from our group.[3a,c,5c] The recovered catalyst was dried in air atmosphere at 393 K for 1 h prior to its storage or further reuse. For sequential catalytic reactions, the experiments were conducted with $Ce_{0.98}Zr_{0.02}O_2$ as the catalyst under the same conditions as those described above. After each run, the catalyst was recovered, washed and dried as previously detailed. In order to evaluate the impact of the solvent on the properties of the catalyst, the as-prepared $Ce_{0.98}Zr_{0.02}O_2$ was subjected to a 42 h treatment in **DMC** under the same conditions to those applied in the catalytic tests. The resulting material was filtered and washed with acetone prior to characterization and further catalytic studies in methoxycarbonylation reactions.

Computational details: Density functional theory (DFT) calculations were carried out with the Vienna ab initio simulation package (VASP, version 5.4.4).[28,29] The generalized gradient approximation (GGA) was used through the Perdew–Burke–Ernzenhof (PBE) functional[30] and the dispersion interactions were accounted through the Grimme D3 approximation.[31] A Hubbard term within the Dudarev approach[32] U = 4.5 eV was added to describe the on-site Coulomb interaction of localized 4f electrons of Ce cations, following previous tests.[33] Projected-augmented wave (PAW) pseudopotentials were used to represent the core electrons whereas valence electrons were expanded in plane waves with a cut-off energy of 500 eV.[34]

Fluorite bulk structure of plain CeO_2 was optimized with a 7×7×7 k-point mesh obtaining a lattice parameter a_{calc} = 5.470 Å (a_{exp} = 5.412 Å).[35] Simulations were performed on (111) and (100) CeO_2 surfaces using slab models with 3 and 4 O–Ce–O trilayers, interleaved by 15 Å vacuum. The dipole correction was applied to avoid the spurious terms due to the asymmetry of the slabs.[36] To simulate the 2% of doping, one Ce cation was substituted by Zr either in surface or in subsurface layer cation positions. The supercells were large enough to avoid the interaction between the adsorbates of neighboring cells and the interaction of more than one

Zr with the adsorbates. The k-points mesh was always denser than 0.3 $Å^{-1}$. In the optimizations, the adsorbates and the topmost layers of the slabs, i.e., 5 atom layers for both facets, were allowed to relax. The gas-phase molecules were optimized inside a box of $20 \times 21 \times 22$ Å. Transition states were identified with the climbing image nudged elastic band (CI-NEB) method[37,38] and refined with the improve dimer method (IDM).[39] The nature of intermediates and transition states were further confirmed by vibrational analysis. All the relevant structures are published in the ioChem-BD database[40] and can be retrieved in the following link: https://dx.doi.org/10.19061/iochem-bd-1-172.

Conflict of interest

The authors declare no conflict of interest.

Keywords: carbamates · ceria · doping · methoxycarbonylation · zirconium

[1] a) G. Scheuerer, *Fortschr. Chem. Forsch.* **1967**, *9*, 254 – 294; b) S. Ray, S. R. Pathak, D. Chaturvedi, *Drugs Future* **2005**, *30*, 161 – 180; c) R. C. Gupta, *Toxicology of Organophosphate and Carbamate Compounds*, Elsevier, **2006**, pp 5 – 24.

[2] Polyurethane Market Size & Share, Global PU Industry Report 2019 – 2025. https://www.grandviewresearch.com/industry-analysis/polyurethane-pu-market (accessed Apr 22, 2020).

[3] a) E. Reixach, N. Bonet, F. X. Rius-Ruiz, S. Wershofen, A. Vidal-Ferran, *Ind. Eng. Chem. Res.* **2010**, *49*, 6362 – 6366; b) X. Zhao, L. Kang, N. Wang, H. An, F. Li, Y. Wang, *Ind. Eng. Chem. Res.* **2012**, *51*, 11335 – 11340; c) E. Reixach, R. M. Haak, S. Wershofen, A. Vidal-Ferran, *Ind. Eng. Chem. Res.* **2012**, *51*, 16165 – 16170; d) S. Wershofen, S. Klein, A. Vidal-Ferran, E. Reixach, F. X. Rius-Ruiz, EP2230228, **2010**; e) T. Dreier, S. Wershofen, A. Vidal-Ferran, R. Haak, WO2014187756A1, 2014; f) Y. Pei, H. Li, H. Liu, Y. Zhang, *Ind. Eng. Chem. Res.* **2011**, *50*, 1955 – 1961.

[4] F. Li, W. Li, J. Li, W. Xue, Y. Wang, X. Zhao, *Appl. Catal. A* **2014**, *475*, 355 – 362.

[5] a) S. Laursen, D. Combita, A. B. Hungría, M. Boronat, A. Corma, *Angew. Chem. Int. Ed.* **2012**, *51*, 4190 – 4193; *Angew. Chem.* **2012**, *124*, 4266 – 4269; b) R. Juárez, A. Corma, H. García, *Pure Appl. Chem.* **2012**, *84*, 685 – 94; c) B. Puértolas, M. Rellán-Piñeiro, J. L. Núñez-Rico, A. P. Amrute, A. Vidal-Ferran, N. López, J. Pérez-Ramírez, S. Wershofen, *ACS Catal.* **2019**, *9*, 7708 – 7720.

[6] R. Juárez, P. Concepción, A. Corma, V. Fornés, H. García, *Angew. Chem. Int. Ed.* **2010**, *49*, 1286 – 1290; *Angew. Chem.* **2010**, *122*, 1308 – 1312.

[7] D.-L. Sun, J.-R. Deng, Z.-S. Chao, *Chem. Cent. J.* **2007**, *1*, 27.

[8] a) X. Guo, Z. Qin, W. Fan, G. Wang, R. Zhao, S. Peng, J. Wang, *Catal. Lett.* **2009**, *128*, 405 – 412; b) Y. Wang, B. Liu, *Catal. Sci. Technol.* **2015**, *5*, 109 – 113; c) S. Wershofen, G. Jaeger, M. Dugal, A. Vidal Ferran, J. L. Núñez Rico, WO2018210711A1, 2018.

[9] N. Lucas, A. P. Amrute, K. Palraj, G. V. Shanbhag, A. Vinu, S. B. Halligudi, *J. Mol. Catal. A: Chem.* **2008**, *295*, 29 – 33.

[10] S. Grego, F. Aricò, P. Tundo, *Pure Appl. Chem.* **2011**, *84*, 695 – 705.

[11] S. Song, J. Shang, H. Wu, Z. Wang, L. Zhang, Y. Zhuang, C. Li, S. Xue, D. Zhao, K. Yang, CN105111106 2015.

[12] S. Rojas-Buzo, P. García-García, A. Corma, *Catal. Sci. Technol.* **2019**, *9*, 146 – 156.

[13] M. Kang, H. Zhou, D. Tang, X. Chen, Y. Guo, N. Zhao, *RSC Adv.* **2019**, *9*, 42474 – 42480.

[14] C. Balaji Gopal, M. García-Melchor, S. C. Lee, Y. Shi, A. Shavorskiy, M. Monti, Z. Guan, R. Sinclair, H. Bluhm, A. Vojvodic, W. C. Chueh, *Nat. Commun.* **2017**, *8*, 15360.

[15] a) A. Trovarelli, C. de Leitenburg, M. Boaro, G. Dolcetti, *Catal. Today* **1999**, *50*, 353 – 367; b) Y. Madier, C. Descorme, A. M. Le Govic, D. Duprez, *J. Phys. Chem. B* **1999**, *103*, 10999 – 11006; c) Q. Fu, H. Saltsburg, M. Flytzani-Stephanopoulos, *Science* **2003**, *301*, 935 – 938; d) Z. Shao, S. M. Haile, *Nature* **2004**, *431*, 170 – 173; e) O. Pozdnyakova, D. Teschner, A. Wootsch, J. Kroehnert, B. Steinhauer, H. Sauer, L. Toth, F. C. Jentoft, A. Knop-Gericke, Z. Paal, R. Schloegl, *J. Catal.* **2006**, *237*, 1 – 16; f) G. Vilé, B. Bridier, J. Wichert, J. Pérez-Ramírez, *Angew. Chem. Int. Ed.* **2012**, *51*, 8620 – 8623; *Angew. Chem.* **2012**, *124*, 8748 – 8751; g) J. Pérez-Ramírez, C. Mondelli, T. Schmidt, O. F. K. Schluter, A. Wolf, L. Mleczko, T. Dreier, *Energy Environ. Sci.* **2011**, *4*, 4786 – 4799; h) A. P. Amrute, C. Mondelli, M. Moser, G. Novell-Leruth, N. López, D. Rosenthal, R. Farra, M. E. Schuster, D. Teschner, T. Schmidt, J. Pérez-Ramírez, *J. Catal.* **2012**, *286*, 287 – 297; i) R. Farra, S. Wrabetz, M. E. Schuster, E. Stotz, N. G. Hamilton, A. P. Amrute, J. Pérez-Ramírez, N. López, D. Teschner, *Phys. Chem. Chem. Phys.* **2013**, *15*, 3454 – 3465; j) A. Trovarelli, *Catal. Rev. Sci. Eng.* **1996**, *38*, 439 – 520; k) T. Montini, M. Melchionna, M. Monai, P. Fornasiero, *Chem. Rev.* **2016**, *116*, 5987 – 6041.

[16] T. Wu, N. López, T. Vegge, H. A. Hansen, *J. Catal.* **2020**, *388*, 1 – 10.

[17] V. Perrichon, A. Laachir, S. Abouarnadasse, O. Touret, G. Blanchard, *Appl. Catal. A* **1995**, *129*, 69 – 82.

[18] R. Farra, M. Eichelbaum, R. Schloegl, L. Szentmiklosi, T. Schmidt, A. P. Amrute, C. Mondelli, J. Pérez-Ramírez, D. Teschner, *J. Catal.* **2013**, *297*, 119 – 127.

[19] a) P. Fornasiero, R. Di Monte, G. R. Rao, J. Kaspar, S. Meriani, A. Trovarelli, M. Graziani, *J. Catal.* **1995**, *151*, 168; b) D. Devaiah, L. H. Reddy, S.-E. Park, B. M. Reddy, *Catal. Rev. Sci. Eng.* **2018**, *60*, 177 – 277.

[20] M. Moser, G. Vilé, S. Colussi, F. Krumeich, D. Teschner, L. Szentmiklósi, A. Trovarelli, J. Pérez-Ramírez, *J. Catal.* **2015**, *331*, 128 – 137.

[21] The complete list of compounds detected in the reaction mixture of the methoxycarbonylation reactions of 2,4-TDA, as well as their chromatographic and spectroscopic characterization can be found in the Supporting Information.

[22] R. Farra, M. García-Melchor, M. Eichelbaum, M. Hashagen, W. Frandsen, J. Allan, F. Girgsdies, L. Szentmiklosi, N. López, D. Teschner, *ACS Catal.* **2013**, *3*, 2256 – 2268.

[23] M. Capdevila-Cortada, G. Vilé, D. Teschner, J. Pérez-Ramírez, N. López, *Appl. Catal. B* **2016**, *197*, 299 – 312.

[24] M. Capdevila-Cortada, N. López, *ACS Catal.* **2015**, *5*, 6473 – 6480.

[25] D. Torres, N. López, F. Illas, R. M. Lambert, *Angew. Chem. Int. Ed.* **2007**, *46*, 2055 – 2058; *Angew. Chem.* **2007**, *119*, 2101 – 2104.

[26] Z. Wang, G. Yang, Z. Zhang, M. Jin, Y. Yin, *ACS Nano* **2016**, *10*, 4559 – 4564.

[27] Q. Li, M. Rellán-Piñeiro, N. Almora-Barrios, M. García-Ratés, I. N. Remediakis, N. López, *Nanoscale* **2017**, *9*, 13089 – 13094.

[28] G. Kresse, J. Furthmueller, *Phys. Rev. B* **1996**, *54*, 11169 – 11186.

[29] G. Kresse, J. Furthmuller, *Comput. Mater. Sci.* **1996**, *6*, 15 – 50.

[30] J. P. Perdew, K. Burke, M. Ernzerhof, *Phys. Rev. Lett.* **1996**, *77*, 3865 – 3868.

[31] S. Grimme, J. Antony, S. Ehrlich, H. Krieg, *J. Chem. Phys.* **2010**, *132*, 154104.

[32] S. L. Dudarev, G. A. Botton, S. Y. Savrasov, C. J. Humphreys, A. P. Sutton, *Phys. Rev. B* **1998**, *57*, 1505 – 1509.

[33] a) S. Fabris, S. de Gironcoli, S. Baroni, G. Vicario, G. Balducci, *Phys. Rev. B* **2005**, *71*, 041102; b) M. Capdevila-Cortada, M. García-Melchor, N. López, *J. Catal.* **2015**, *327*, 58 – 64; c) M. Capdevila-Cortada, Z. Lodziana, N. López, *ACS Catal.* **2016**, *6*, 8370 – 8379.

[34] G. Kresse, D. Joubert, *Phys. Rev. B* **1999**, *59*, 1758 – 1775.

[35] E. A. Kümmerle, G. Heger, *J. Solid State Chem.* **1999**, *147*, 485 – 500.

[36] G. Makov, M. C. Payne, *Phys. Rev. B* **1995**, *51*, 4014 – 4022.

[37] G. Henkelman, H. Jónsson, *J. Chem. Phys.* **2000**, *113*, 9978 – 9985.

[38] G. Henkelman, B. P. Uberuaga, H. Jonsson, *J. Chem. Phys.* **2000**, *113*, 9901 – 9904.

[39] A. Heyden, A. T. Bell, F. J. Keil, *J. Chem. Phys.* **2005**, *123*, 224101.

[40] M. Álvarez-Moreno, C. de Graaf, N. López, F. Maseras, J. M. Poblet, C. Bo, *J. Chem. Inf. Model.* **2015**, *55*, 95 – 103.